EUROPHYSICS LETTERS 1 April 2006

Europhys. Lett., **74** (1), pp. 103–109 (2006)
DOI: 10.1209/epl/i2006-10003-3

Electrical-field–induced curvature increase on a drop of conducting liquid

M. Bienia[1], M. Vallade[1], C. Quilliet[1] and F. Mugele[2]

[1] *Laboratoire de Spectrométrie Physique UMR CNRS-UJF*
140 avenue de la Physique, 38400 Saint-Martin-d'Hères, France
[2] *University of Twente, Physics of Complex Fluids*
P.O. Box 217, 7500 AE Enschede, The Netherlands

received 29 July 2005; accepted in final form 9 February 2006
published online 1 March 2006

PACS. 68.03.-g – Gas-liquid and vacuum-liquid interfaces.
PACS. 68.08.Bc – Wetting.
PACS. 83.60.Np – Effects of electric and magnetic fields.

Abstract. – We present an analytical approach using conformal mapping to the free-boundary problem of the shape of a liquid drop submitted to a strong electrical field, as encountered in electrowetting systems. In agreement with recent numerical calculations, we show that both the curvature of the surface profile and the electric field diverge algebraically close to the three-phase line. The algebraic exponents agree with the numerical results. We show analytically that the local contact angle remains equal to Young's angle, independent of the applied voltage. Furthermore, we present experimental evidence of a curvature increase close to the contact line.

Introduction. – The contact angle change of a drop of conducting liquid on an insulating solid under the influence of an external electrical field, called electrowetting, has become a field of strong interest in the area of wetting in the last twenty years [1,2]. The applications of this phenomenon range from the variable focus lens [3–5] to microfluidics (controlled displacement, rupture and coalescence of droplets [6–9]), *via* pixel units for electronic paper [10,11]. Recent fundamental work is largely related to the study of limiting phenomena such as contact angle saturation [12–15] and triple-line instability leading to droplet expulsion [16,17]. While the origin of contact angle saturation has yet to be determined in detail, most of the suggested explanations attribute it to the divergence of electric fields close to the contact line [1,2]. The classical electrowetting theory neglects these effects: by balancing the gain in electrostatic energy and the additional surface energy one obtains the following relation between the change of the macroscopic *apparent* contact angle, the so-called Lippmann angle θ_L, and the applied voltage V [2,18–21]:

$$\cos\theta_L(V) \;=\; \cos\theta_Y + \frac{1}{2}\frac{\mathcal{C}V^2}{\gamma} = \cos\theta_Y + \eta. \tag{1}$$

Here θ_Y is Young's contact angle, $\mathcal{C} = \varepsilon_0\varepsilon_r/d$ is the capacitance per unit area between the droplet and the counter-electrode underneath the insulating layer (thickness d, dielectric

constant ε_r). γ is the surface tension of the liquid and η is a dimensionless electrowetting number which measures the relative importance of electrostatic energy (per unit area) and surface tension([1]). Since the total electrostatic energy gain is proportional to the solid-liquid interfacial area, eq. (1) can also be viewed as the result of an *effective* reduction of the solid-liquid interfacial energy $\gamma_{sl}^{eff}(V) = \gamma_{sl,0} - CV^2/2$.

Close to the three-phase line, however, the description given above fails: field enhancement due to electrostatic edge effects gives rise to a strong Maxwell stress deforming the droplet surface. In a recent study, Buehrle *et al.* [21] used numerical calculations to determine the equilibrium shape of the droplet. In this paper, we present an analytical approximation using conformal mapping that allows to reproduce the main results much more elegantly. Furthermore, we present experimental evidence of a curvature increase close to the contact line in agreement with the theoretical predictions.

Theory. – Let us consider a drop of a perfectly conducting liquid on top of a dielectric solid of thickness d. An electrical potential V is applied between the drop and a counter-electrode underneath the solid. In the vicinity of the contact line, the surface profile at zero voltage can be approximated by a wedge with an opening angle $\alpha = \theta_Y$. For this fixed geometry, the electrostatic field distribution was calculated exactly using conformal mapping by Vallet *et al.* [16]. The electric field was found to diverge close to the contact line. In mechanical equilibrium, this gives rise to a diverging Maxwell stress acting on the droplet surface. As a result, the surface profile is distorted which, in turn, affects the field distribution. The challenge is thus to calculate the electrical field *and* the drop shape simultaneously for a general free-boundary problem. Buehrle *et al.* [21] used an iterative numerical method to solve this problem for a two-dimensional droplet. Their calculations show that an electric-field–induced curvature appears close to the triple line over a length scale of the order of the thickness of the insulating film and that the contact angle goes asymptotically to the (zero field) Young angle when approaching this line.

In the following we show that these results can also be derived (at least in the low-field limit) from analytical considerations and conformal mapping techniques.

In order to allow a direct comparison with the numerical simulations in [21] and for the sake of simplicity, we restrict ourselves to a 2D system, and all relative permittivities ε_r are taken to be equal to 1. The liquid is considered a perfect conductor (*i.e.* the electric field vanishes inside the liquid). *A priori*, the shape of the interface is not known. However, there exists a conformal mapping function $w(z)$ of the complex plane ($z = x + iy$) onto itself ($w = u + iv$) which transforms the two electrodes at potential 0 and V into two electrodes of an infinite parallel-plate capacitor (see fig. 1) [23].

The reciprocal mapping $z(w)$ has a derivative of the general form:

$$\frac{\mathrm{d}z}{\mathrm{d}w} = F(w)e^{i\psi(w)}, \tag{2}$$

where $F(w)$ and $\psi(w)$ denote, respectively, the modulus and argument of $\frac{\mathrm{d}z}{\mathrm{d}w}$. In the following, we shall use dimensionless quantities: the lengths will be expressed in units of d/π and the voltages in units of V/π.

The functions $x(u), y(u)$ at constant v provide a parametrical representation of the equipotential curves, whereas the electrical-field components are given by [23]

$$E_x(u) - iE_y(u) = \frac{i}{\left(\frac{dz}{dw}\right)} = \frac{i}{\dot{x}(u) + i\dot{y}(u)}, \tag{3}$$

([1])Instead of minimizing the total energy of the droplet, the same result can also be obtained using the Maxwell stress tensor formalism, as introduced in the context of electrowetting by Jones *et al.* [22].

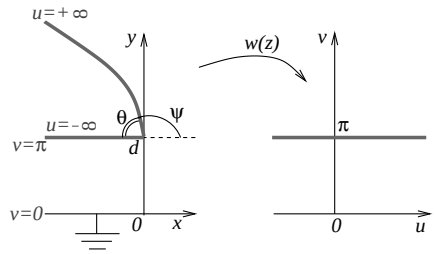

Fig. 1 – Conformal mapping that transforms the edge of liquid into a planar electrode. The analytical function $w(z)$ maps the x-axis onto the $v = 0$ line, and the boundaries of the drop onto the $v = \pi$ line.

where

$$\dot{x}(u) = \left.\frac{\partial x}{\partial u}\right|_v , \qquad \dot{y}(u) = \left.\frac{\partial y}{\partial u}\right|_v . \tag{4}$$

According to eq. (2), for constant v we also have

$$F(u) = \sqrt{\dot{x}^2(u) + \dot{y}^2(u)}, \tag{5}$$

$$\tan\psi(u) = \frac{\dot{y}(u)}{\dot{x}(u)} = \frac{\mathrm{d}y}{\mathrm{d}x}. \tag{6}$$

In real space $\psi(u)$ corresponds to the angle of the equipotential (*i.e.* interface profile) with the x-axis. In mechanical equilibrium, this angle is a function of the height above the substrate. Its value is coupled to the local electric field by the equilibrium condition between the Maxwell stress and the Laplace pressure [21]:

$$\gamma\kappa(r) + \frac{\varepsilon_0}{2}E^2(r) = 0, \tag{7}$$

where $\kappa(r)$ is the mean curvature at point r.

In order to transform the capillary equation into the transformed space, we first express both the curvature and the electric field in terms of $F(u)$ and $\psi(u)$:

$$\kappa(u) = \frac{\ddot{x}\dot{y} - \ddot{y}\dot{x}}{(\dot{x}^2 + \dot{y}^2)^{3/2}} = -\frac{\partial\psi}{\partial u}\frac{1}{F(u)}, \tag{8}$$

$$|E(u)|^2 = \frac{1}{(\dot{x}^2 + \dot{y}^2)} = \frac{1}{F(u)^2}. \tag{9}$$

Hence the capillary equation (7) can be simply written as

$$\frac{\partial\psi}{\partial u} = \frac{\eta}{\pi F(u)}, \tag{10}$$

where η is the dimensionless electrowetting number defined above. Formally, we can integrate eq. (10) to obtain

$$\psi(u) = \psi_\infty - \frac{\eta}{\pi}\int_u^\infty \frac{\mathrm{d}u'}{F(u')}, \tag{11}$$

where ψ_∞ corresponds to the slope of the surface far away from the triple line, *i.e.* $\psi_\infty = \pi - \theta_L$.

In the following, we will seek a solution that holds for small values of η. To do so, we start with the well-known solution for $\eta = 0$. In this case, we know that the $\psi(u)$ is constant along

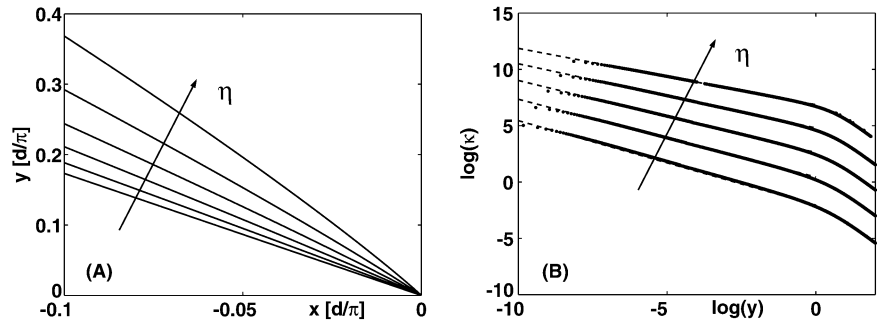

Fig. 2 – (A) Liquid/air profiles calculated with the analytical model, for $\theta_L = 60°$, in reduced units. Far from the contact line, all the profiles have the same slope, corresponding to Lippmann's angle. (B) curvature as a function of height, with, respectively, $\eta = 0.2$ to 1 by steps of 0.2 and $\theta_L = 60°$; $\theta_Y = 72.5$, 84.3, 99.7, 107.5 and 120°. The dashed lines are the power law behavior expected from [16, 21], calculated with Young's angle, and equal to, respectively, -0.75, -0.69, -0.64, -0.57 and -0.5. For the sake of clarity, (B) curves are shifted on the vertical axis by $+2$. Far from the contact line, all the curves have the same slope of -2 (see text).

the liquid/air interface ($\psi \equiv \psi_0 = \pi - \theta_Y$). The droplet profile is thus given by a perfect wedge with zero curvature. For this geometry the conformal transformation $z_0(w)$ is known [16]: $\mathrm{d}z_0/\mathrm{d}w = F_0(w)e^{i\psi_0(w)} = (e^w + 1)^\alpha$, where $\alpha = \psi_0/\pi$. The first-order perturbation to ψ can be obtained by using the zeroth-order mapping function $F_0 = (e^u - 1)^\alpha$ in eq. (11):

$$\psi(u) \;=\; \psi_\infty - \frac{\eta}{\pi}\int_u^\infty \frac{\mathrm{d}u'}{(e^{u'} - 1)^\alpha}, \tag{12}$$

assuming that $F(u)$ is a non-singular function at $\eta = 0$. The integral in this equation is the Eulerian Beta function $B_a(x, y)$. Using a parametric representation, we find

$$\theta(u) \;=\; \theta_L + \frac{\eta}{\pi} B_{e^{-u}}(\alpha, 1 - \alpha), \tag{13}$$

$$s(u) \;=\; (e^u - 1)^{1+\alpha} F(1, 1 + \alpha, 2 + \alpha, 1 - e^u)/(1 + \alpha), \tag{14}$$

where $F(a, b, c, x)$ is the hypergeometric function and $s(u) = \int_0^u F_0(u')\mathrm{d}u'$ represents the curvilinear abscissa along the liquid/air interface.

Figure 2(A) represents liquid/air profiles obtained for $\theta_L = 60°$, with η ranging from 0.2 to 1. Young's angle ranges from 72.5 to 120°. We also plotted the calculated 2D curvature according to eq. (8) for these profiles in fig. 2(B). Far away from the triple line ($y \gg 1$), the curvature displays an algebraic behavior with an exponent of 2 corresponding to $E \propto 1/y$, as expected from basic electrostatics. Upon approaching the triple line (around $y \approx 1$) the curvature crosses over to another algebraic region with a smaller exponent, indicating a divergence of the curvature, and hence of the electric field. The power law exponents are consistent with the result obtained in [16, 21] (cf. dashed lines), and are equal to -0.75, -0.69, -0.64, -0.57 and -0.5. It is remarkable that this agreement holds even for a value of $\eta = 1$ despite the approximation in eq. (12). A qualitative explanation for this agreement can be found by considering the local slope angle at the triple line. Another important result of [21] was that the local slope at the contact line is equal to θ_Y, *i.e.* $\psi(u = 0) = \pi - \theta_Y$. Differentiating

eq. (1) with respect to η one gets for $\eta = 0$: $\partial\psi_\infty/\partial\eta|_{\eta=0} = 1/\sin\theta_Y$, and

$$\begin{aligned}\psi(0) \approx \psi_0 + \eta \left.\frac{\partial\psi(0)}{\partial\eta}\right|_{\eta=0} &= \psi_0 + \eta\left(\left.\frac{\partial\psi_\infty}{\partial\eta}\right|_{\eta=0} - \frac{1}{\pi}\int_0^\infty \frac{\mathrm{d}u'}{(e^{u'}-1)^\alpha}\right) \\ &= \psi_0 + \eta\left(\frac{1}{\sin\theta_Y} - \frac{1}{\sin(\pi\alpha)}\right). \end{aligned} \tag{15}$$

Since $\pi\alpha = \psi_0 = \pi - \theta_Y$, the term in brackets vanishes, and we obtain

$$\psi(0) = \psi_0, \tag{16}$$

i.e. the local contact angle at the triple line remains unaffected by the applied voltage. To the first order in η, we thus recover the result of [21] that the electrostatic force acting on the triple line vanishes. The forces inducing the contact angle reduction in electrowetting are distributed over a range on the order of d rather than acting directly on the triple line, as suggested by the simplest derivation of eq. (1). They cannot be described by a simple voltage-dependent effective surface tension. This is related to the long-range character of electrostatic interactions.

In real systems, the divergence of the curvature and the electric field will be cut off at short length scales. Molecular interactions will distort the actual surface profile within the range of the disjoining pressure. Furthermore, the perfect conduction assumption of the liquid breaks down on the scale of the Debye length, which is on the order of a few Angströms for typical salt concentration in electrowetting. Finally, the actual dielectric permittivities of the system have to be considered [24] .

Experiments. – In order to verify the theoretical predictions, we measured the curvature of liquid droplets close to the triple line using high resolution video microscopy. To facilitate the optical observation, we used insulators consisting of 150, 300 and 450 μm thick glass layers ($\varepsilon_r = 3.8$). The top plate is covered by a layer of several hundreds of Angströms of spin-coated Teflon AF (Dupont) to ensure hydrophobicity. The counter-electrode, which is grounded, is a thick ITO-covered glass plate. A drop of the conducting liquid guarantees a homogeneous electrical contact between the glass and the electrode.

The conducting liquid is $BMIMBF_4$ (Sigma), an ionic liquid of interfacial energy $62\,\mathrm{mN\,m^{-1}}$ and density $\rho = 1.22\,\mathrm{kg\,L^{-1}}$, which results in droplets sizes inferior to the capillary length ($\kappa^{-1} = 2.3\,\mathrm{mm}$). The droplet volumes $\mathcal{V}$ are 3 to 6 μL giving rise to a range of Bond numbers $Bo = g\rho\mathcal{V}^{2/3}/\gamma = 0.4$ to 0.6. A thin platinum electrode brings the drop to high alternative electrical potential at 10 kHz frequency.

The drop is illuminated using an optical fiber and an opaque screen. Pictures of 1024×1280 pixels resolution are acquired by a 16 bits video-camera mounted on the binocular. Side view images of the drop are obtained by a mirror tilted by 45°. Voltage ramps ranging in 0–700 V for 150 μm samples, 0–900 V for the 300 μm samples and 0–1200 V for the 450 μm at a frequency of 10 kHz are applied to the droplets, corresponding to a range of $\eta = 0$–0.5.

The curvature is measured using interface profiles extracted from side view images, assuming that the system is axisymmetric. For each voltage, several pictures from two independent experiments were taken. The analysis starts 20 pixels above the contact line to avoid possible artifacts due to the finite size of the pixels, which result in an apparent rounding of the tip of the drop. We chose $r(y)$ as the coordinates of the profile, in order to prevent numerical divergences in the curvature calculations in case of contact angle of the drop larger than 90°. We obtain $r(y)$ by detecting the inflection point in intensity variation from white (background) to black (drop). The 3D curvature is calculated using finite differences and box averaging. We

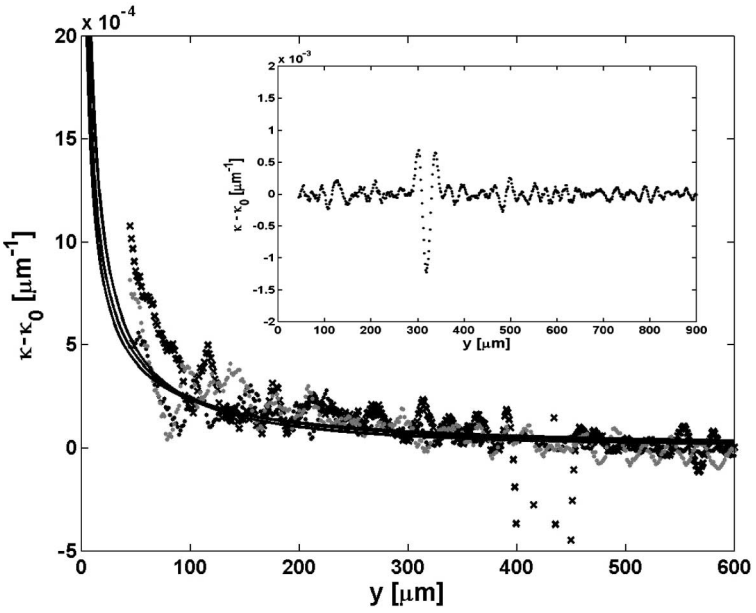

Fig. 3 – Excess curvature in μm^{-1} as a function of height y in μm: black dots 700 V, black crosses 900 V, gray dots 1200 V. The lines are theoretical predictions for each set of experiments, respectively from bottom to top, obtained with $\theta_L = 70^\circ$ and $\eta = 0.5$ ($\theta_Y = 99^\circ$). Inset: excess curvature $\kappa - \kappa_0$ at 0 V, as a function of height in microns. These values are in good agreement with expected curvatures for spherical caps of the same volume and contact angle as in the experiments within 4%. The large variation around 300 μm is due to the presence of the electrode coming out of the drop, in one of the experiments. A linear trend attributed to gravity, obtained by a linear fit in the range of macroscopic curvature and whose order of magnitude is in agreement with a rough estimate of hydrostatic pressure, is substracted from all the data.

tested this procedure using a spherical cap with 1% noise, and it resulted in a shift of 3% in the value of the curvature we calculated compared to the actual value [25].

The excess curvature $\kappa(y) - \kappa_0$ as a function of height y is shown fig. 3, at high voltage for the 3 different thicknesses (inset: $\kappa(y) - \kappa_0$ as a function of height y for 0 V). κ_0 is the "macroscopic" curvature, *i.e.* far from the contact line. The latter is obtained by averaging the curvature in the range 500 μm and higher above the substrate. The 3 sets of experiments correspond to $\eta = 0.5$, $\theta_L = 70^\circ$, and $\theta_Y = 99^\circ$. For the sake of comparison, the results of the analytical model for the same parameters are plotted along with the experimental results. Despite the noise amplification induced by the derivation process, we detect a curvature increase close to the triple line on the high potential curves. This deviation is clearly seen until $y \simeq 100\,\mu$m above the triple line.

Conclusion. – Recent numerical results predict a curvature increase near the triple line for a drop of conducting liquid at high electrical potentials, due to strong electrical fields near the triple line. We present an analytical approach to this problem in the case of low electrical fields, which leads to the same conclusions. We show that the horizontal component of electrostatic forces vanishes at the three-phase line, resulting in Young's angle exactly at the triple line, for a perfectly conducting liquid. Similar behavior is observed for colloids [26].

Our present experimental results show that a curvature increase can actually be detected for a drop at high electrical potential. The variation is clearly seen up to a distance of the order of a hundred microns above the contact line, and its amplitude is 10% of the asymptotic curvature. These results are in qualitative agreement with our theoretical model.

* * *

MB would like to thank the EURODOC program for financial support.

REFERENCES

[1] Mugele F. and Baret J.-C., *J. Phys. Condens. Matter*, **17** (2005) R705.
[2] Quilliet C. and Berge B., *Curr. Opin. Colloid Interface Sci.*, **6** (2001) 34.
[3] Berge B. and Peseux J., *Eur. Phys. J. E*, **3** (1999) 159.
[4] Yang S., Krupenkin T. N., Mach P. and Chandross E., *Adv. Mater.*, **15** (2003) 940.
[5] Kuiper S. and Hendriks B. H. W., *Appl. Phys. Lett.*, **85** (2004) 1128.
[6] Srinivasan V., Pamula V. K. and Fair R. B., *Lab Chip*, **4** (2004) 310.
[7] Cho S.-K., Fan S.-K., Moon H. and Kim C.-J., *IEEE*, (2002) 32.
[8] Cho S.-K., Moon H., Fowler J. and Kim C.-J., *Micro-Electro-Mechanical-Systems MEMS, 2001 ASME International Mechanical Engineering Congress and Exposition, New York*, Vol. **3** (American Society of Mechanical Engineers, New York) 2001, p. 207.
[9] Washizu M., Kawabata T., Kurosawa O. and Suzuki S., *Transactions of the Institute of Electronics, Information and Communication Engineers C*, **J83-C** (2000) 1.
[10] Hayes R. and Feenstra B., *Nature*, **425** (2003) 383.
[11] Roques-Carmes T., Hayes R. A., Feenstra B. J. and Schlangen L. J. M., *J. Appl. Phys.*, **95** (2004) 4389.
[12] Quinn A., Sedev R. and Ralston J., *J. Phys. Chem. B*, **107** (2003) 1163.
[13] Vallet M., PhD Thesis, Université Joseph Fourier (1997).
[14] Verheijen H. J. J. and Prins M. W. J., *Langmuir*, **15** (1999) 6616.
[15] Papathanasiou A. G. and Boudouvis A. G., *Appl. Phys. Lett.*, **86** (2005) 164102.
[16] Vallet M., Vallade M. and Berge B., *Eur. Phys. J. B*, **11** (1999) 583.
[17] Mugele F. and Herminghaus S., *Appl. Phys. Lett.*, **81** (2002) 2303.
[18] Lippmann G., *Ann. Chim. Phys.*, **5** (1875) 494.
[19] Froumkine A., *Actual. Sci. Ind.*, **373** (1936) 5.
[20] Berge B., *C. R. Acad. Sci. III*, **317** (1993) 157.
[21] Buehrle J., Herminghaus S. and Mugele F., *Phys. Rev. Lett.*, **91** (2003) 086101.
[22] Jones T. B., *J. Micromech. Microengin.*, **15** (2005) 1184.
[23] Lavrentief M. and Chabat B., *Méthodes de la théorie des fonctions d'une variable complexe* (Éditions Mir, Moscou) 1977.
[24] Chou T., *Phys. Rev. Lett.*, **87** (2001) 106101.
[25] Bienia M., PhD Thesis, Université Joseph Fourier (2005).
[26] Oettel M., Dominguez A. and Dietrich S., *Phys. Rev. E*, **71** (2005) 051401.